Photon emission statistics and photon tracking in single-molecule spectroscopy of molecular aggregates

Bloemsma, E. A.; Knoester, J.

Published in:
Journal of Chemical Physics

DOI:
10.1063/1.4719210

Photon emission statistics and photon tracking in single-molecule spectroscopy of molecular aggregates: Dimers and trimers

E. A. Bloemsma and J. Knoester[a)]
Centre for Theoretical Physics and Zernike Institute for Advanced Materials, University of Groningen, Nijenborgh 4, 9747 AG Groningen, The Netherlands

(Received 27 January 2012; accepted 3 May 2012; published online 13 June 2012)

Based on the generating function formalism, we investigate broadband photon statistics of emission for single dimers and trimers driven by a continuous monochromatic laser field. In particular, we study the first and second moments of the emission statistics, which are the fluorescence excitation line shape and Mandel's Q parameter. Numerical results for this line shape and the Q parameter versus laser frequency in the limit of long measurement times are obtained. We show that in the limit of small Rabi frequencies and laser frequencies close to resonance with one of the one-exciton states, the results for the line shape and Q parameter reduce to those of a two-level monomer. For laser frequencies halfway the transition frequency of a two-exciton state, the photon bunching effect associated with two-photon absorption processes is observed. This super-Poissonian peak is characterized in terms of the ratio between the two-photon absorption line shape and the underlying two-level monomer line shapes. Upon increasing the Rabi frequency, the Q parameter shows a transition from super- to sub- to super-Poissonian statistics. Results of broadband photon statistics are also discussed in the context of a transition (frequency) resolved photon detection scheme, photon tracking, which provides a greater insight in the different physical processes that occur in the multi-level systems.
 [http://dx.doi.org/10.1063/1.4719210]

I. INTRODUCTION

The optical properties and dynamics of excitons in low-dimensional aggregates of interacting molecules form a rich research area, spanning a wide range of systems composed of (bio)organic molecules.[1] These include, for instance, the class of J-aggregates of synthetic cyanine dye molecules,[2–6] with applications as photosensitizers, but also the large family of natural light-harvesting complexes of chlorophyll molecules that occur in bacteria and higher plants,[7,8] as well as crystals and thin layers of conjugated oligomers and polymers used in current organic optoelectronic devices.[9]

Generally, low-dimensional molecular aggregates are complex systems, whose excitonic properties result from an interplay of intermolecular excitation transfer (resonance) interactions, static disorder caused by interactions with frozen (slow) degrees of freedom in the environment of the aggregate, as well as dynamic disorder, caused by faster degrees of freedom interacting with the excitons. Optical spectroscopy offers a large tool box to study this interplay. The vast majority of optical spectroscopies applied to these complex systems consist of bulk measurements, where since the late 1980s in particular nonlinear optical techniques, such as photon echoes,[10–13] pump-probe,[14–17] and, most recently, two-dimensional correlation spectroscopy,[8,18–22] have opened new ways to unravel details hidden in linear spectroscopy. In parallel to these developments, also single-molecule spectroscopy (SMS), introduced around 1990,[23,24] has proven a powerful experimental technique to study complex molecular systems.[25–29] SMS allows one to directly address single systems of interest in a –possibly– heterogeneous ensemble, thereby avoiding the ensemble averaging that necessarily takes place in bulk experiments and allowing one to look directly under the inhomogeneous line shapes measured in ensemble spectra. SMS experiments performed on single bacteriochlorophyll aggregates,[30] terylene dimers,[31] tetraphenoxy-perylene diimide trimers,[32] and single aggregates of amphi-pseudoisocyanine[33] have indeed revealed that interesting details on collective optical transitions are hidden underneath the ensemble average.

The analysis of the discrete data stream of spontaneously emitted photons obtained in SMS experiments has generated an interesting theoretical field of research (see Refs. 34–36 and references therein). Here, the main effort has been to analyze the photon stream generated by a single molecule interacting with its environment. In general, photon emission streams obey a probability distribution $P_n(\omega_L, T)$ that describes the possibility of detecting a number of photons n in a certain time interval T for a particular laser frequency ω_L. Both in theoretical and experimental work, the focus lies on determining and interpreting the first and second moments of this distribution. More specific, the first moment, denoted $I(\omega_L, T)$, is defined as the average number of photons emitted (broadband detection) from the system per unit time for particular frequencies of the incoming light. For measurement times longer than any dynamical time scale present in the system, the line shape $I(\omega_L, T)$ is identical to the (fluorescence) excitation spectrum. The second moment of the distribution is conveniently represented by the Mandel parameter,[37] denoted $Q(\omega_L, T)$, which provides a measure for

[a)]Electronic mail: j.knoester@rug.nl.

the variance of the number of emitted photons. Here, negative (positive) values of Q imply that the variance of the distribution is decreased (increased) relative to the Poisson distribution. Such statistics is typically referred to as sub-Poissonian (super-Poissonian) and is indicative of photon antibunching (bunching) behavior. For Q equal to zero, the case of purely Poissonian statistics is recovered. We note that Mandel's Q parameter is closely related to the two-point correlation function, or fluorescence intensity correlation function, $g_2(t)$ that describes the correlation between arrival times of emitted photons.[35]

The different approaches used to model the photon emission data streams[35,36,38–40] have provided us with a good understanding of the mechanisms at work that account for the fluctuations in the photon counts. Examples include the effect of blinking caused by a long-lived triplet state in the molecule,[41–43] the phenomenon of photon antibunching inherent to the quantum nature of radiation and observed in the fluorescence of a single two-level molecule in (near)-resonance with the laser field,[37,39,44,45] and photon bunching which may result, for instance, from spectral diffusion.[35,38,40,46–49] However, thus far only very few theoretical studies have been devoted to the analysis of photon statistics for assemblies of coupled molecules. Jang and Silbey[50,51] derived a theoretical framework for the single-molecule line shapes of multichromophoric systems and applied it to a model of the B850 ring in the light-harvesting complex 2 of purple bacteria. Sanda and Mukamel[52] calculated the two-point fluorescence intensity correlation function $g^{(2)}(t)$ and the time-dependence of Mandel's Q parameter $Q(t)$ for a strongly pumped dimer undergoing Gaussian-Markovian frequency fluctuations.

In this paper, we present the framework for calculating photon emission statistics of an aggregate described by the Frenkel exciton model[53,54] interacting with a classical continuous monochromatic laser field. To extract photon statistics, the generalized Bloch equations (GBE) formalism developed by Zheng and Brown[39,40] is adapted. Within this method, the ordinary optical Bloch equations governing the dynamics of the system and its interaction with the laser field are rewritten using generating functions[55] from which statistical moments of the photon counting process follow naturally. The equations for the generating functions are exact within the rotating wave approximation and the limits set by the Hamiltonian. This method has already been applied successfully to single two-level chromophores[39,40,46–49,56,57] and their extension to multi-level quantum systems,[58,59] and has also been used by Sanda and Mukamel.[52] Using numerical methods, we apply the general equations to investigate the fluorescence excitation line shape (we will refer to this, for short, as the line shape) and Mandel's Q parameter as a function of laser frequency in the limit of long measurement times, i.e., much longer than any dynamical time scale present, for both dimers and trimers of interacting molecules.

Our analysis for the dimer shows that laser frequencies close to resonance with one of the one-exciton transitions lead to sub-Poissonian statistics as a result of photon antibunching. This is expected, because in this frequency region the dimer can to a good approximation be regarded as an effective two-level system. For laser frequencies halfway the transition frequencies of the individual two-level monomers, however, it turns out that the photon statistics is more complicated. Hettich *et al.*[31] measured both the fluorescence excitation spectrum and autocorrelation function $g^{(2)}(t)$ for single pairs of strongly interacting terylene molecules embedded in a *para*-terphenyl crystal. For intense laser illumination a new peak was found in the excitation spectrum, halfway the two one-exciton transition frequencies of the dimer. This peak arises from the significant enhancement of the resonant two-photon absorption and corresponding two-photon emission process under intense laser fields. The corresponding autocorrelation function $g^{(2)}(t)$ showed that the statistics was super-Poissonian, revealing the signature of photon bunching. We will show that upon increasing the laser intensity, the photon statistics in this region undergoes a transition from super- to sub-Poissonian and back again to super-Poissonian. For larger systems, in particular for the trimer, similar effects occur.

The photon counting measurements from SMS and their statistical analysis and interpretation have focused mainly on broadband photon detection schemes, in which the color of the emitted photons has been ignored. Two of the exceptions are the study by Gopich and Szabo[60] concerning the distribution of the number of donor and acceptor photons from single molecule Förster resonance energy transfer measurements and the work of Bel, Zheng, and Brown,[58] in which statistical moments were calculated for multi-level quantum systems, based on an extension of the generating function method. Using extended generating functions, we determine a general scheme for calculating statistical moments of transition resolved (frequency resolved) photons emitted from a molecular aggregate. This photon tracking method provides us with a better insight in the physical processes that occur under illumination.

This paper is organized as follows. In Sec. II A we present the Frenkel exciton model Hamiltonian for an aggregate of interacting molecules. Section II B describes the conversion of the resulting optical Bloch equations to the set of generalized Bloch equations and reviews the extraction of broadband photon emission statistics from this formalism. Section II C is devoted to the description of the photon tracking method. In Sec. III we present numerical results for the fluorescence excitation line shape and Q parameter of several specific dimer and trimer systems and discuss these results in the context of the photon tracking method and the well-known results for the single two-level chromophore.[37,49] Finally, we present our conclusions in Sec. IV. Several technical details are given in the Appendix.

II. THEORETICAL FRAMEWORK

A. Model Hamiltonian

The optical response of molecular aggregates is well described by the Frenkel exciton model. In this model, the monomers are treated as effective two-level systems that interact with each other via strong resonance dipole-dipole couplings. Allowing for site dependent transition frequencies and

interactions (i.e, disorder), the corresponding Hamiltonian within the Heitler-London approximation[53,54] reads ($\hbar = 1$)

$$\hat{H}_{agg} = \sum_n \omega_n b_n^\dagger b_n + \sum_{n,m} J_{nm} b_n^\dagger b_m. \tag{1}$$

Here, ω_n denotes the transition frequency of the nth monomer, J_{nm} is the matrix element of the resonant transfer interaction between monomers n and m, and $b_n^\dagger$ (b_n) is the Pauli creation (annihilation) operator of an excitation on monomer n. The operators satisfy the (anti-)commutation relations

$$[b_n, b_m^\dagger] = \delta_{nm}(1 - 2b_m^\dagger b_n), \quad b_n^\dagger b_n^\dagger = b_n b_n = 0. \tag{2}$$

These relations express the fact that the two-level monomer can carry at most one excitation.

For an aggregate of N molecules, diagonalizing the Hamiltonian yields 2^N eigenstates, denoted $|i\rangle (i = 1, 2, \ldots, 2^N)$, and their energies E_i. Because the Hamiltonian conserves the total number of excitons, these eigenstates can be classified into manifolds of multi-exciton states according to the number of excitation quanta they share. Therefore, in the exciton state basis $\{|i\rangle\}$ the aggregate can be treated as a 2^N energy-level diagram consisting of $(N + 1)$ manifolds. Here, the lowest manifold contains only the ground state of the aggregate, which in the Heitler-London approximation is the state with all molecules in their ground state. The corresponding energy is set $E_1 = 0$. The next lowest manifold contains the N one-exciton states, which share a single excitation quantum, the third lowest manifold the $N(N - 1)/2$ two-exciton states that share two excitations, etc.

The interaction of a classical continuous wave laser field of frequency ω_L and electric field amplitude $\mathbf{E}_0$ with the optical transitions of the aggregates is in the dipole approximation (aggregate small compared to an optical wavelength) given by

$$\hat{H}_{int}(t) = -\hat{\mathbf{M}} \cdot \mathbf{E}_0 \cos \omega_L t, \tag{3}$$

where $\hat{\mathbf{M}}$ denotes the transition dipole operator of the aggregate, which is given by the sum of single monomer dipole operators, $\hat{\mathbf{M}} = \sum_{n=1}^N \boldsymbol{\mu}_n (b_n^\dagger + b_n)$, with $\boldsymbol{\mu}_n$ indicating the transition dipole matrix element (assumed real) between the ground and excited state of monomer n. As $\hat{\mathbf{M}}$ is a sum of single monomer operators, in the exciton eigenstate basis the only possible non-zero matrix elements of $\hat{\mathbf{M}}$ are those corresponding to transitions between states that lie in adjacent exciton manifolds. The Rabi frequencies corresponding to these transitions are defined as

$$\Omega_{ij} \equiv -\frac{\mathbf{M}_{ij} \cdot \mathbf{E}_0}{2}, \tag{4}$$

with $\mathbf{M}_{ij} = \langle i|\hat{\mathbf{M}}|j\rangle$.

The dynamics of the aggregate interacting with a classical laser field can be described in terms of the density operator $\rho(t)$, whose evolution is determined by the Liouville-von Neumann equation.[61] To account for spontaneous emission events, we add phenomenological damping terms to this equation leading to the following 2^{2N} equations for the (multi-) exciton populations $\rho_{ii}(t)$ and coherences $\rho_{ij}(t) (i \neq j)$

$$\left(\frac{d\hat{\rho}(t)}{dt}\right)_{ii} = -\imath[\hat{H}(t), \hat{\rho}(t)]_{ii} + \sum_j{}' \Gamma_{ij}\rho_{jj}(t) - \sum_j{}'' \Gamma_{ji}\rho_{ii}(t), \tag{5a}$$

$$\left(\frac{d\hat{\rho}(t)}{dt}\right)_{ij} = -\imath[\hat{H}(t), \hat{\rho}(t)]_{ij} - \frac{1}{2}(\Gamma_i + \Gamma_j)\rho_{ij}(t), \tag{5b}$$

with $\imath$ denoting the imaginary unit. Here, $\hat{H}(t) = \hat{H}_{agg} + \hat{H}_{int}(t)$ is the total Hamiltonian for an aggregate interacting with a classical laser field, $\sum_j{}' (\sum_j{}'')$ denotes the sum over j for which $E_j > E_i$ ($E_j < E_i$), Γ_{ij} gives the rate at which population decays from level $|j\rangle$ to $|i\rangle$ due to a spontaneous emission event, and Γ_i denotes the total decay rate of population out of level $|i\rangle$, i.e., $\Gamma_i = \sum_j{}'' \Gamma_{ji}$. The decay rate Γ_{ij} can be described by Einstein's A coefficient

$$\Gamma_{ij} = \frac{1}{3\pi\epsilon}\left(\frac{E_j - E_i}{c}\right)^3 |\mathbf{M}_{ij}|^2, \tag{6}$$

with ϵ the permittivity of the surrounding medium and c the vacuum speed of light.

B. Generating function formalism and photon statistics

Although the set of 2^{2N} optical Bloch equations as given by Eqs. (5) suffices to determine all dynamics of the aggregate, statistical moments of the spontaneous photon emission process cannot be obtained directly from these equations. As pointed out previously,[40,55] information about these statistics is contained in the generating function

$$G_{ij}(s, t) = \sum_{n=0}^{\infty} \sigma_{ij}^{(n)}(t) s^n. \tag{7}$$

Here, s is an auxiliary variable and the $\sigma_{ij}^{(n)}(t)$ denote the generalized populations ($i = j$) or coherences ($i \neq j$), which are defined by $\rho_{ij}(t) = \sum_n \sigma_{ij}^{(n)}(t)$, where n denotes the number of photons spontaneously emitted prior to time t. Therefore, $\sigma_{ij}^{(n)}(t)$ can be interpreted as the density operator of systems which have spontaneously emitted n photons prior to time t. Using arguments given elsewhere,[39,56] the equations of motion for $G_{ij}(s, t)$ follow from Eqs. (5) as

$$\left(\frac{d\hat{G}(s,t)}{dt}\right)_{ii} = -\imath[\hat{H}(t), \hat{G}(s,t)]_{ii} + s\sum_j{}' \Gamma_{ij} G_{jj}(s,t) - \sum_j{}'' \Gamma_{ji} G_{ii}(s,t), \tag{8a}$$

$$\left(\frac{d\hat{G}(s,t)}{dt}\right)_{ij} = -\imath\left[\hat{H}(t), \hat{G}(s,t)\right]_{ij} - \frac{1}{2}(\Gamma_i + \Gamma_j) G_{ij}(s,t). \tag{8b}$$

These equations differ from those for the total density operator (Eqs. (5)) only in the fact that terms describing population increase of a level due to radiative decay out of a higher

energy level are accompanied with an extra factor s. It is the auxiliary variable s that allows us to extract photon statistics from these equations, as will be shown below.

To obtain the solution to the set of equations for $G_{ij}(s, t)$, we invoke the rotating wave approximation (RWA) (Ref. 62) and introduce slowly changing variables to ensure that the resulting equations have only time independent and real coefficients. These variables are of the form

$$C_{ij}^{\pm}(s,t) = \frac{\imath^{-\frac{1}{2}\pm\frac{1}{2}}}{2}(G_{ij}(s,t)e^{-\imath\omega_{ij}t} \pm G_{ji}(s,t)e^{\imath\omega_{ij}t}), \quad (9a)$$

$$P_{kl}^{\pm}(s,t) = \frac{1}{2}(G_{kk}(s,t) \pm G_{ll}(s,t)). \quad (9b)$$

Here, i and j run from $1, \ldots, 2^{2N}$ with $i < j$, $\{k, l\} = \{\{1, 2\}, \{3, 4\}, \ldots, \{2^N - 1, 2^N\}\}$, and ω_{ij} is defined as zero if i and j represent levels that lie in the same exciton band, ω_L if they represent levels in adjacent bands, $2\omega_L$ for levels that are two exciton bands apart, etc. The resulting set of equations, often referred to as the set of generalized Bloch equations, can be cast in the form

$$\dot{\mathbf{X}}(s,t) = M(s)\mathbf{X}(s,t), \quad (10)$$

where $\mathbf{X}(s,t) = (C_{ij}^{+}(s,t); C_{ij}^{-}(s,t); P_{ij}^{-}(s,t); P_{ij}^{+}(s,t))^T$ is the column vector containing all the slowly changing variables, the dot reflects the time derivative, and $M(s)$ denotes a $2^{2N} \times 2^{2N}$ time independent matrix. The solution to Eq. (10) is given by

$$\mathbf{X}(s,t) = e^{M(s)t}\mathbf{X}_0(s,t_0). \quad (11)$$

Throughout this paper, the initial condition is chosen to reflect the aggregate's ground state, i.e., $\mathbf{X}_0(s, t_0 = 0) = (0; 0; 1/2, 0, \ldots, 0; 1/2, 0, \ldots, 0)$.

Once the solution to the generalized Bloch equations is known, information on photon statistics is obtained through the following equality:[40]

$$2\sum_{\{k,l\}} P_{kl}^{+}(s,t) = \sum_{n=0}^{\infty}\sum_{i=1}^{2^N}\sigma_{ii}^{n}(t)s^n = \sum_{n=0}^{\infty}P_n(t)s^n. \quad (12)$$

Here, $P_n(t)$ is identified as the probability that n photons have been emitted in the time interval $[0, t]$. The two quantities of interest in this paper are the fluorescence excitation line shape $I(\omega_L) \equiv \lim_{t\to\infty}\frac{\langle n(t)\rangle}{t}$ (hereafter, referred to as the line shape) and the Mandel parameter $Q(\omega_L, t) \equiv \frac{\langle n^2(t)\rangle - \langle n(t)\rangle^2}{\langle n(t)\rangle} - 1$,[45] where $\langle \ldots \rangle$ denotes the average over the spontaneous photon emission process. Using Eq. (12), $I(\omega_L)$ may be expressed as

$$I(\omega_L) = \lim_{t\to\infty}\frac{2\frac{\partial}{\partial s}\sum_{\{k,l\}}P_{kl}^{+}(s,t)|_{s=1}}{t}, \quad (13)$$

and $Q(\omega_L, t)$ as

$$Q(\omega_L,t) = \frac{2\frac{\partial^2}{\partial s^2}\sum_{\{k,l\}}P_{kl}^{+}(s,t)|_{s=1} - \left(2\frac{\partial}{\partial s}\sum_{\{k,l\}}P_{kl}^{+}(s,t)|_{s=1}\right)^2}{2\frac{\partial}{\partial s}\sum_{\{k,l\}}P_{kl}^{+}(s,t)|_{s=1}}. \quad (14)$$

The Q parameter is defined so that $Q = 0$ corresponds to Poissonian statistics, whereas the values $Q < 0$ ($Q > 0$) are referred to as sub(super)-Poissonian statistics. Sub-Poissonian behavior is associated with the effect of photon antibunching, whereas super-Poissonian statistics is related to photon bunching. In general, Mandel's Q parameter is a function of both the measurement time t and the laser frequency ω_L; throughout this paper we will focus only on the limit $t \to \infty$ of long measurement times.

C. Photon tracking

The formalism derived in Secs. II A and II B determines broadband photon statistics, i.e., statistics of all photons spontaneously emitted from the aggregate, independent of their frequencies. With minor modifications, it is possible to calculate statistics of photons originating from a specific transition in the aggregate.

Let $\mathbf{n} = (n_1, n_2, \ldots, n_\kappa)$ be a vector, where each element n_i gives the total number of photons emitted due to a single radiatively allowed transition and let $\mathbf{s} = (s_1, s_2, \ldots s_\kappa)$ be the vector of auxiliary variables that correspond to these transitions. In order to find the statistics, we introduce the generating function

$$\widetilde{G}_{ij}(\mathbf{s},t) = \sum_{n_1,n_2,\ldots,n_\kappa}\widetilde{\sigma}_{ij}^{(\mathbf{n})}(t)\left[\prod_{l=1}^{\kappa}s_l^{n_l}\right]. \quad (15)$$

Here, each element n_i of the summation runs from zero to infinity. The main difference between the generating function for broadband photon statistics (Eq. (7)) and the one given here, is that $\widetilde{\sigma}_{ij}^{(\mathbf{n})}(t)$ explicitly depends on the number of photons n_i emitted within each allowed transition, whereas $\sigma_{ij}^{(n)}(t)$ (Eq. (7)) depends solely on the total number of emitted photons n ($n = \sum_i n_i$).

The set of equations for the generating functions $\widetilde{G}_{ij}(\mathbf{s}, t)$ are given by

$$\left(\frac{d\widetilde{G}(\mathbf{s},t)}{dt}\right)_{ii} = -\imath[\hat{H}(t), \widetilde{G}(\mathbf{s},t)]_{ii} + s_{ji}\sum_{j}{}'\Gamma_{ij}\widetilde{G}_{jj}(\mathbf{s},t) - \sum_{j}{}''\Gamma_{ji}\widetilde{G}_{ii}(\mathbf{s},t), \quad (16a)$$

$$\left(\frac{d\widetilde{G}(\mathbf{s},t)}{dt}\right)_{ij} = -\imath[\hat{H}(t), \widetilde{G}(\mathbf{s},t)]_{ij} - \frac{1}{2}(\Gamma_i + \Gamma_j)\widetilde{G}_{ij}(\mathbf{s},t). \quad (16b)$$

Here, s_{ji} is the auxiliary variable related to the specific radiative transition $|j\rangle \to |i\rangle$. The solution to Eqs. (16) is obtained in the same way as before, that is, one introduces a set of slowly changing variables similar to Eqs. (9) and applies the RWA. The statistics of photons due to a specific allowed transition is then obtained from the derivative of the solution to these equations with respect to the auxiliary variable associated with that transition. For instance, the average number of photons emitted as a result of the transition $|j\rangle \to |i\rangle$ reads

$$\langle n_{ji}(t)\rangle = 2\frac{\partial}{\partial s_{ji}}\sum_{\{k,l\}}P_{kl}^{+}(\mathbf{s},t)|_{\mathbf{s}=(1,1,\ldots,1)}. \quad (17)$$

III. NUMERICAL ANALYSIS

This section is devoted to the numerical analysis of the line shape and Q parameter in the long measurement time limit for dimers and trimers. The dimer consists of two two-level monomers with transition frequencies ω_1 and ω_2, that interact through an intermolecular excitation transfer interaction J, leading to collective optical transitions. For explicitness, we will choose J to be positive. The Appendix provides the exciton eigenstates and energies together with all system parameters Ω_{ij} and Γ_{ij}, expressed in their single monomer quantities $\Omega_0 \equiv -\frac{\boldsymbol{\mu}\cdot\mathbf{E}_0}{2}$ and $\Gamma_0 \equiv \frac{\mu^2}{3\pi\epsilon}(\frac{\omega_0}{c})^3$ ($\omega_0 \equiv \frac{\omega_1+\omega_2}{2}$), respectively. Also the set of generalized Bloch equations for the dimer as derived from Eqs. (8) and (9) is listed there. As an example of a larger system, we will discuss photon statistics of a chain consisting of three identical two-level monomers with dipole-dipole interactions.

A. Homogeneous dimer

We first consider the special case of a completely homogeneous dimer where both monomers have the same transition frequency ω_0. Furthermore, we assume the transition dipole vectors $\boldsymbol{\mu}_1$ and $\boldsymbol{\mu}_2$ to be parallel. It then follows directly from Eqs. (A3) and (A4) that $\Gamma_{g-} = \Gamma_{-e} = \Omega_{g-} = \Omega_{-e} = 0$, so that the anti-symmetric one-exciton state $|-\rangle$ cannot absorb nor emit photons; thus, the system can be represented as an effective three-level system characterized by its ground state $|g\rangle$, the symmetric one-exciton state $|+\rangle$ and the two-exciton state $|e\rangle$, with Rabi frequencies $\Omega_{g+} = \Omega_{+e} \equiv \Omega_+$ and spontaneous decay rates Γ_{g+}, Γ_{+e} (see Fig. 1).

1. Small Rabi frequency limit

Figure 2 presents the numerical results for $I(\omega_L)$ and $Q(\omega_L)$ in the limit of small Rabi frequencies, $|\Omega_+| \ll \Gamma_{+g}$, Γ_{e+}. As is observed, $I(\omega_L)$ consists of a single peak centered around the one-exciton transition frequency $E_+ = \omega_0 + J$. This peak is explained as follows. There are two contributions to $I(\omega_L)$: spontaneous emission out of the $|+\rangle$ state and out of the two-exciton state $|e\rangle$. In the limit considered here, where $|\Omega_+| \ll \Gamma_{+g}$, the excitation probability of the two-exciton state is negligible and its contribution to the emission spectrum may be ignored. Near the peak at $\omega_L \approx E_+$, the off-resonance nature of two-exciton creation, either from the $|+\rangle$ state by one-photon excitation or from the ground state $|g\rangle$ via two-photon excitation, further reduces the possible contribution from the $|e\rangle$ state. Using the photon tracking method introduced in Sec. II C, we calculated this contribution, taking $R = \langle n_{e+}\rangle/(\langle n_{e+}\rangle + \langle n_{+g}\rangle)$ as a characteristic measure. For $(\omega_L - \omega_0) = J$ and $\Omega_0 = -1 \times 10^{-3}J$, this gives $R \approx 2.7 \times 10^{-7}$, which shows that near the one-exciton resonance the contribution to $I(\omega_L)$ of photons emitted as a result of the excitation of the $|e\rangle$ state is indeed negligibly small. Therefore, when using a laser with low intensity and tuned close to the one-exciton resonance, the dimer can effectively be treated as a two-level monomer. This may be corroborated further by considering the line shape for the two-level system[49]

$$I_{TLS}(\omega_L) = \frac{\Gamma\Omega^2}{\Gamma^2 + 2\Omega^2 + 4\Delta^2}. \tag{18}$$

Here, the symbols have their usual meaning, Γ is the spontaneous decay rate, $\Omega \equiv -\frac{\mu|\mathbf{E}_0|}{\hbar}$ is the Rabi frequency, and Δ indicates the detuning of the laser away from the resonance frequency of the two-level system. Identifying these parameters with the values appropriate for the $|g\rangle \rightarrow |+\rangle$ transition in the dimer, we indeed obtain a line shape which cannot be distinguished from the peak in Fig. 2(a).

We now turn to discussing the results for $Q(\omega_L)$ in Fig. 2(b). Based on the foregoing discussion, for $\omega_L \approx \omega_0$

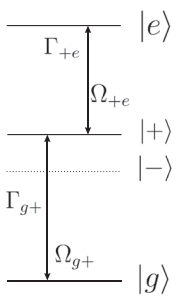

FIG. 1. Level diagram of the dimer. In the special case of a homogeneous dimer, the dotted anti-symmetric state $|-\rangle$ is optically dark and the dimer can be regarded as an effective three-level system.

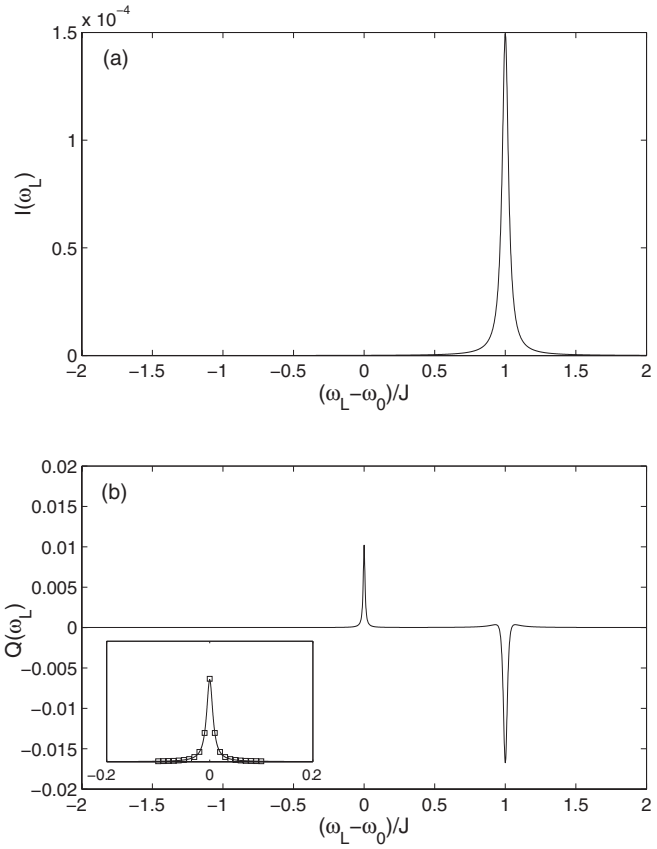

FIG. 2. (a) $I(\omega_L)$ and (b) $Q(\omega_L)$ versus $(\omega_L - \omega_0)/J$ in the small Rabi frequency limit for the homogeneous dimer. Chosen parameters are $\omega_0 = 10J$, $\Gamma_0 = 2 \times 10^{-2}J$, $\Omega_0 = -1 \times 10^{-3}J$. Calculated parameters based on Eqs. (A3) and (A4) are $\Gamma_{g+} = 5.3 \times 10^{-2}J$, $\Gamma_{+e} = 2.9 \times 10^{-2}J$, $\Omega_+ = -1.4 \times 10^{-3}J$. (Inset) Our numerical results for the super-Poissonian peak (solid line) compared to the results derived from Eq. (20).

$+ J$ the behavior of $Q(\omega_L)$ is expected to reproduce that of a single two-level monomer[49]

$$Q_{TLS}(\omega_L) = -\frac{2\Omega^2(3\Gamma^2 - 4\Delta^2)}{(\Gamma^2 + 2\Omega^2 + 4\Delta^2)^2} \tag{19}$$

with the appropriate parameters. Indeed, the numerical results for $Q(\omega_L)$ are in perfect agreement with Eq. (19). Therefore, for $\omega_L \approx E_+$, the photon statistics is sub-Poissonian. We point out that in general $Q_{TLS}(\omega_L)$ has a second-derivativelike structure in the sense that its value is negative for resonant laser frequencies ($\Delta = 0$), but turns positive (when $\Delta^2 > (4/3)\Gamma^2$) before approaching zero in the limit $\Delta \to \infty$. This second-derivative structure can, for example, clearly be observed in Fig. 3(b).

In contrast to the above, for frequencies $\omega_L \approx \omega_0$ the observed behavior of $Q(\omega_L)$ in Fig. 2(b) cannot be explained from a simple two-level system picture. The positive peak of $Q(\omega_L)$, i.e., super-Poissonian statistics, indicates the presence of photon bunching. Physically, this effect is a consequence of the $|e\rangle$ state and is explained as follows. Of the two possible processes mentioned above to populate the $|e\rangle$ state, at $\omega_L \approx \omega_0$ only the two-photon absorption process from the ground state is resonant. Therefore, this process is expected to dominate the creation of the $|e\rangle$ state. From the $|e\rangle$ state, the system decays to the $|+\rangle$ state through the spontaneous emission of a single photon. In the $|+\rangle$ state, the system can further decay to the $|g\rangle$ state by the emission of another photon or return to the $|e\rangle$ state by absorbing another photon from the laser beam. As the latter process is not resonant and $|\Omega_+| \ll \Gamma_{g+}, \Gamma_{+e}$, after populating the $|e\rangle$ state the system will decay to the $|g\rangle$ state by the emission of two photons rapidly after each other compared to $|\Omega_+|^{-1}$. This effect leads to photon bunching.

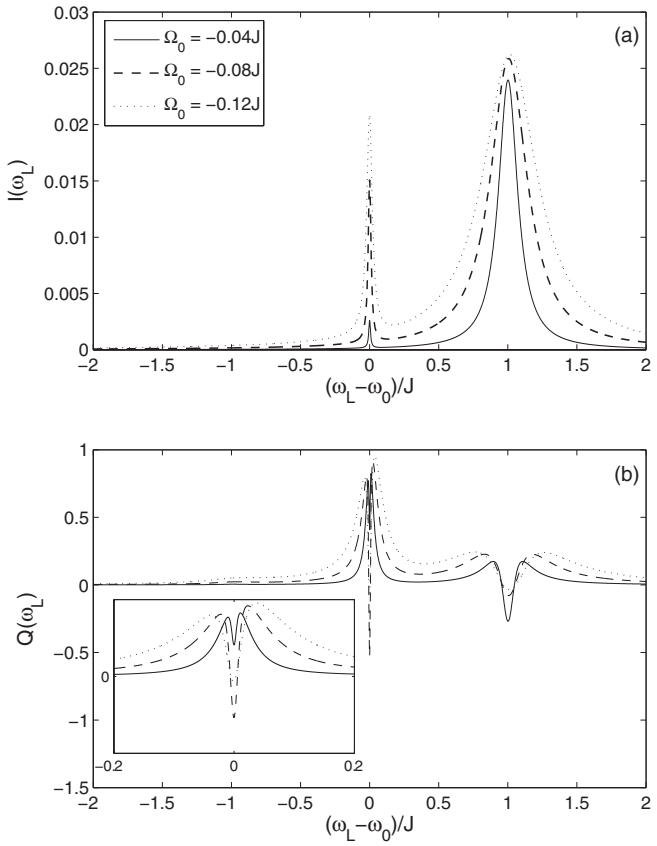

FIG. 3. (a) $I(\omega_L)$ and (b) $Q(\omega_L)$ for the homogeneous dimer as a function of $(\omega_L - \omega_0)/J$ for intermediate Rabi frequencies, $\Omega_0 = -4 \times 10^{-2}J$, $-8 \times 10^{-2}J$, and $-1.2 \times 10^{-1}J$. Parameters are the same as those of Fig. 2, leading to $\Omega_+ = -5.7 \times 10^{-2}J$, $-1.1 \times 10^{-1}J$, and $-1.7 \times 10^{-1}J$, respectively. (Inset) Transition from super- to sub-Poissonian behavior in more detail.

Using photon tracking we calculated $R \approx 5.1 \times 10^{-3}$ for $\omega_L = \omega_0$. This shows that even for laser frequencies in resonance with the two-photon absorption process, the $|g\rangle \Leftrightarrow |+\rangle$ cycle is the dominant process to occur for the Rabi frequencies considered here. However, the contribution of this two-level system process to $Q(\omega_L)$ is very small, $Q(\omega_L) \propto \frac{\Omega_+^2}{J^2} \ll 1$, as seen from Eq. (19). Therefore, the $|g\rangle \Leftrightarrow |e\rangle$ cycle is the process that determines the behavior of $Q(\omega_L)$ for $\omega_L \approx \omega_0$, which leads to the observed super-Poissonian statistics. It should be stressed that $I(\omega_L)$ does not show clear signatures of the two-photon absorption process. Thus, $Q(\omega_L)$ provides complementary information on the role of two-exciton states that cannot be deduced from $I(\omega_L)$.

The latter may be demonstrated further by considering the super-Poissonian behavior in more detail (inset of Fig. 2(b)). To this end, we note that studies of single molecules undergoing a stochastic spectral diffusion (Kubo-Anderson) process have demonstrated that (in certain limits) super-Poissonian statistics may be expressed in terms of a ratio of line shapes involved.[38,46] In analogy to this, we found that if $\omega_L \approx \omega_0$ and $|\Omega_+| \ll \Gamma_{g+}, \Gamma_{+e} \ll J$, the observed super-Poissonian peak is indistinguishable from the expression

$$Q(\omega_L) = \frac{I_2(\omega_L)}{2I_+(\omega_L)}. \tag{20}$$

Here, $I_+(\omega_L)$ is the two-level monomer line shape (Eq. (18)) corresponding to the $|g\rangle \to |+\rangle$ transition in the dimer and $I_2(\omega_L)$ is the two-photon absorption line shape, which, in second-order perturbation theory, can be expressed as[63]

$$I_2(\omega_L) = \left| \sum_k \frac{\Omega_{ke}\Omega_{gk}}{\omega_k - \omega_L} \right|^2 \frac{\Gamma_e}{\Gamma_e^2 + 4(\omega_e - 2\omega_L)^2}. \tag{21}$$

The summation extends over all intermediate states $|k\rangle$ (in our case $|k\rangle = |+\rangle$ only), ω_k is the transition frequency between the ground state and $|k\rangle$, and Γ_e^{-1} is the lifetime of the two-exciton state $|e\rangle$. Thus, the super-Poissonian peak of the homogeneous dimer is found to be approximately Lorentzian with FWHM Γ_{+e} and maximum value $Q_{max} \approx 2\Omega_+^2/(\Gamma_{g+}\Gamma_{+e})$.

The above discussion shows that in the low intensity limit, the Q parameter in principle can be used as a tool to address the role of the two-exciton state in the dimer. We point out that such information is accessible in an experimental situation, provided that enough photon emission events are recorded to accurately measure Q_{max}. Because the number of photon events per unit time resulting from excitation of the two-exciton state is obviously small for low laser intensities, this requires in general long measurement times. These times, however, are limited by the fact that after a number of excitation cycles the molecules are destroyed by the light to which

they are exposed (photobleaching). Therefore, to experimentally gain information on the two-exciton state at low laser intensities requires the use of molecules that are not too sensitive to photobleaching (i.e., can go through a large number of excitation cycles).

2. Intermediate Rabi frequencies

To further study the effects of the two-exciton state on photon statistics, the single monomer Rabi frequency Ω_0 was increased, leading to faster Rabi oscillations $|\Omega_+| \approx \Gamma_{g+}$, Γ_{+e}. Figure 3 displays $I(\omega_L)$ and $Q(\omega_L)$ for the homogeneous dimer for three different values of Ω_0. For laser frequencies $\omega_L \approx \omega_0 + J$, $I(\omega_L)$ and $Q(\omega_L)$ show characteristics also found in the small Rabi frequency limit. The essential differences with the low-intensity limit is that the widths of spectral features in $I(\omega_L)$ and $Q(\omega_L)$ clearly undergo power broadening; in addition, their maxima (minima) also appear to be shifted with respect to the two-level system approximation introduced in Sec. III A 1. Numerically, this shift may be estimated to be $\Delta_s \approx \Omega_+^2/2J$. This shift finds its origin in a shift of the one-exciton state $|+\rangle$, due to the effective coupling between the $|+\rangle$ and the $|e\rangle$ states induced by the strong laser fields.

For $\omega_L \approx \omega_0$ both $I(\omega_L)$ and $Q(\omega_L)$ fundamentally differ from the results found in the small Rabi frequency limit. $I(\omega_L)$ shows a peak that increases with increasing field intensity Ω_0, which was not seen for small Rabi frequencies. This peak is a direct manifestation of the significant enhancement of the resonant two-photon absorption process upon increasing laser intensities.[61] Indeed, the appearance of such a peak under intense laser illumination has also been observed experimentally for two strongly coupled terylene molecules by Hettich *et al.* in Ref. 31. Using the photon tracking method we calculated the average number of emitted photons per unit time for the different possible transitions, taking $\omega_L = \omega_0$ and $\Omega_0 = -0.08$. This yielded $\langle n_{+g}\rangle \approx 7.7 \times 10^{-3}$ and $\langle n_{e+}\rangle \approx 7.3 \times 10^{-3}$, which gives $R \approx 0.49$. These data suggest that not only the $|e\rangle$ state is easily populated due to a two-photon absorption process, but also that the system decays from the $|e\rangle$ state via the $|+\rangle$ state to the $|g\rangle$ state by the emission of two photons rather then re-excite from the $|+\rangle$ state to the $|e\rangle$ state by absorbing a photon. Thus, the $|g\rangle \Leftrightarrow |e\rangle$ cycle is the dominant process to occur in the dimer at intermediate Rabi frequencies for laser frequencies $\omega_L \approx \omega_0$.

For $Q(\omega_L)$ an interesting phenomenon occurs when $\omega_L \approx \omega_0$. It is seen from Fig. 3(b) that $Q(\omega_L)$ has a second-derivativelike shape, quite similar to that for a two-level monomer but clearly distinct from the Lorentzian shape observed for small Rabi frequencies. Moreover, its minimum value (occurring at $\omega_L = \omega_0$) indicates that exactly at the two-photon resonance, photon statistics can either be super- or sub-Poissonian, depending on the strength of the applied laser field Ω_0, in contrary to the purely super-Poissonian statistics obtained for slow Rabi oscillations. We note that in the experiment by Hettich *et al.* it was found that under intense laser illumination photon statistics connected to the simultaneous excitation of both strongly coupled terylene molecules in a dimer is super-Poissonian.[31] Our results, however, imply that such statistics sensitively depend on the strength of the applied laser field and that in general it can give rise both to super- and sub-Poissonian behavior.

The observation of sub-Poissonian statistics, i.e., the fact that the emitted photons are correlated in their arrival times, can be explained as follows. Once the dimer is excited into the $|e\rangle$ state, it emits two photons (not correlated) and collapses into the ground state. Before the dimer can emit another photon, it first needs to be re-excited to the $|e\rangle$ state through two-photon absorption (dominant process), which takes a finite amount of time. Hence, emission events of pairs of photons are stretched on the time axis, which leads to sub-Poissonian statistics. This effect disappears if the Rabi frequencies become too large or too small compared to the spontaneous decay rates. The above reasoning then determines a region of possible values for the strength of the applied laser field for which sub-Poissonian statistics can be observed. For the model parameters used to generate Fig. 3 we find numerically that this region is given by $0.05J \lessapprox |\Omega_0| \lessapprox 0.12J$.

B. Inhomogeneous dimer

The case of a completely homogeneous dimer will not occur in practice, because the host matrix of dimers and larger aggregates usually exhibits structural disorder (liquid solvents, glasses and protein matrices are frequently occurring hosts), which leads to differences in the transition frequencies of the individual molecules. Here, we will assume these frequencies to be constant on the time scale of the experiment (static disorder) and refer to them as ω_1 and ω_2. The quantity $\sigma \equiv \left|\frac{\omega_1-\omega_2}{2}\right|$ then serves as the characteristic measure for the amount of inhomogeneity within the dimer and $\omega_0 \equiv \frac{\omega_1+\omega_2}{2}$ denotes the average transition frequency. The eigenstates, emission constants, and Rabi frequencies for general ω_1 and ω_2 are given in the Appendix. The aim of this section is to analyze the effect of the inhomogeneity on $I(\omega_L)$ and $Q(\omega_L)$.

Figures 4(a) and 4(c) show $I(\omega_L)$ and $Q(\omega_L)$, respectively, in the limit of small inhomogeneity, $\sigma \ll J$, and small Rabi frequencies, $|\Omega_{ij}| \ll \Gamma_{ij}$ (we assumed equal transition dipoles $\boldsymbol{\mu}_1 = \boldsymbol{\mu}_2$). $I(\omega_L)$ then consists of two Lorentzians, centered at the one-exciton transition frequencies $E_\pm$. We have verified, using the parameter values corresponding to the $|g\rangle \rightarrow |\pm\rangle$ transitions, that the observed Lorentzian line shapes are in agreement with Eq. (18). For $Q(\omega_L)$, we observe close to the one-exciton transition frequencies the second-derivative structures with sub-Poissonian behavior for resonant laser frequencies, as dictated by Eq. (19), while at $\omega_L \approx \omega_0$ we find a Lorentzian shaped super-Poissonian peak caused by the presence of the two-exciton state. As the inhomogeneity induces a non-zero dipole moment between the ground state and the one-exciton state $|-\rangle$ (which is dipole-forbidden in the homogeneous dimer), the super-Poissonian peak is better approximated by a generalization of Eq. (20),

$$Q(\omega_L) = \frac{I_2(\omega_L)}{2[I_+(\omega_L) + I_-(\omega_L)]}, \quad \omega_L \approx \omega_0. \tag{22}$$

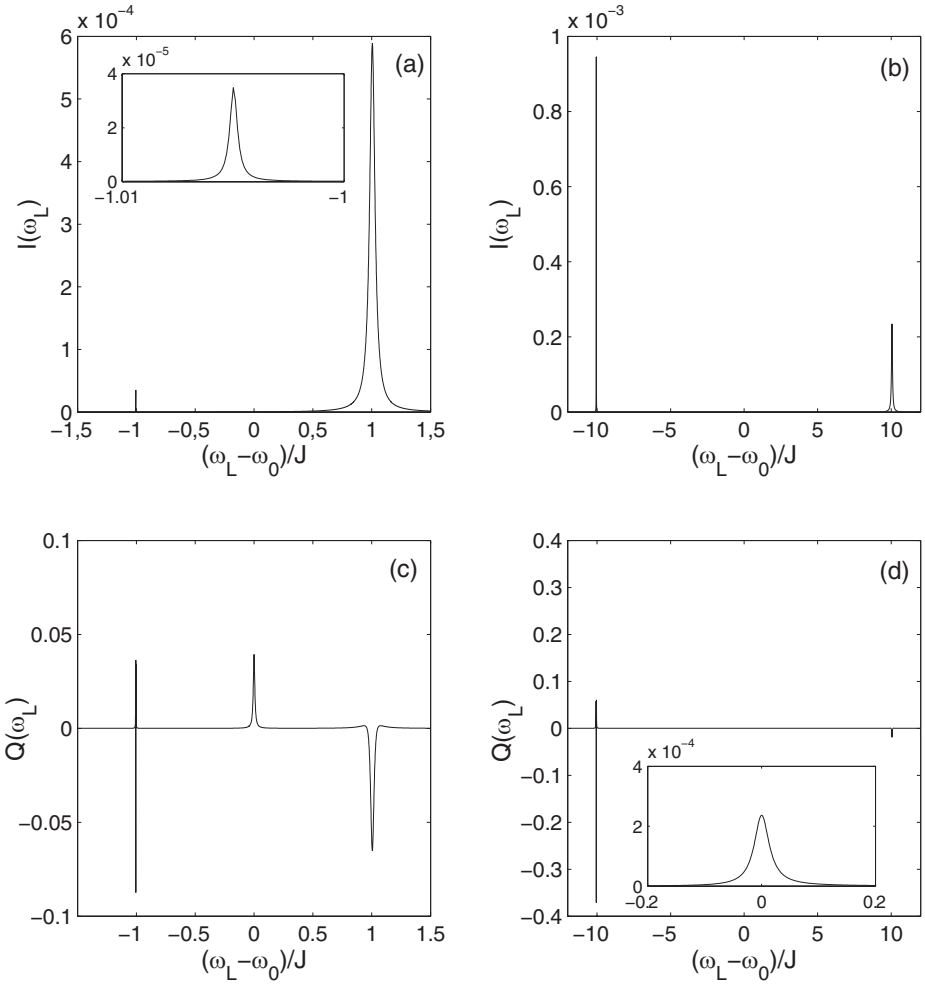

FIG. 4. Plots of $I(\omega_L)$ and $Q(\omega_L)$ versus $(\omega_L - \omega_0)/J$ for the dimer in both limits of inhomogeneity. Panels (a) and (c) present the data for small inhomogeneity, with parameter choices $\omega_1 = 10J$, $\omega_2 = 10.2J$ (i.e., $\sigma = 0.1J$), $\Gamma_0 = 2 \times 10^{-2}J$, and $\Omega_0 = -2 \times 10^{-3}J$. From this it follows that $\Gamma_{g+} = 5.3 \times 10^{-2}J$, $\Gamma_{+e} = 2.9 \times 10^{-2}J$, $\Gamma_{g-} = 7.2 \times 10^{-5}J$, $\Gamma_{-e} = 1.3 \times 10^{-4}J$, $\Omega_{g+} = \Omega_{+e} = -2.8 \times 10^{-3}J$, and $\Omega_{g-} = \Omega_{-e} = -1.4 \times 10^{-4}J$. Panels (b) and (d) present data for large inhomogeneity, with parameter choices $\omega_1 = 10J$, $\omega_2 = 30J$ (i.e., $\sigma = 10J$), $\Gamma_0 = 2 \times 10^{-2}J$, and $\Omega_0 = -2 \times 10^{-3}J$. From this we have $\Gamma_{g+} = 7.5 \times 10^{-2}J$, $\Gamma_{+e} = 2.7 \times 10^{-3}J$, $\Gamma_{g-} = 2.2 \times 10^{-3}J$, $\Gamma_{-e} = 6.1 \times 10^{-2}J$, $\Omega_{g+} = \Omega_{+e} = -2.1 \times 10^{-3}J$, and $\Omega_{g-} = \Omega_{-e} = -1.9 \times 10^{-3}J$. Inset (a): details of the $|g\rangle \rightarrow |-\rangle$ transition line shape. Inset (d): observation of the small super-Poissonian peak for $\omega_L \approx \omega_0$.

We have confirmed numerically that the super-Poissonian peak, observed in Fig. 4(c), is in perfect agreement with Eq. (22).

Figures 4(b) and 4(d) present $I(\omega_L)$ and $Q(\omega_L)$, respectively, in the opposite limit $\sigma \gg J$ of large inhomogeneity. In this limit, the one-exciton states reduce to the excited states of the uncoupled molecules and any collective optical properties of the dimer are expected to vanish. The observed $I(\omega_L)$ indeed confirms this idea, as it consists of two Lorentzians centered roughly at the transition frequencies of the single molecules and in perfect agreement with Eq. (18) for the single monomer parameters. Note that the difference in linewidth and height of the two Lorentzians is a direct consequence of the transition energy dependence of the spontaneous decay rates Γ_{g-} and Γ_{g+} (Eq. (6)). In accordance, $Q(\omega_L)$ shows the characteristic second-derivative structure, where statistics is sub-Poissonian for laser frequencies resonant with one of the monomer transition frequencies. The inset of Fig. 4(d) shows $Q(\omega_L)$ for $\omega_L \approx \omega_0$. The super-Poissonian peak, characteristic for the influence of the two-exciton state, is still observed, although its maximum value decreased by two orders of magnitude with respect to the limit of small inhomogeneity.

In Fig. 5, we further analyze the maximum value Q_{max} of the observed super-Poissonian peak as a function of the disorder parameter σ. The two graphs correspond to the cases where the energy dependence of the spontaneous decay rates is taken into account (main plot) and where it is neglected (inset). For both graphs and all disorder strengths, we find that the numerically calculated data (squares) is in excellent agreement with the results obtained from Eq. (22) (solid line). The distinction between the two different regimes of small and large inhomogeneity is clearly seen in Fig. 5. In the limit $\sigma \ll J$, Q_{max} is roughly independent of disorder. This is expected, as to first order in J the eigenstates of the dimer are identical to those of the homogeneous dimer. In the opposite limit of $\sigma \gg J$, it follows from Eq. (22) that, when the dependence of Γ_{ij} on the transition energy is neglected, Q_{max} depends on the disorder strength σ through the power law $Q_{max} = 2(\frac{\Omega_0}{\Gamma_0})^2 (\sigma/J)^{-2}$. If the energy dependence of the decay rates is taken into account, no strict power law behavior

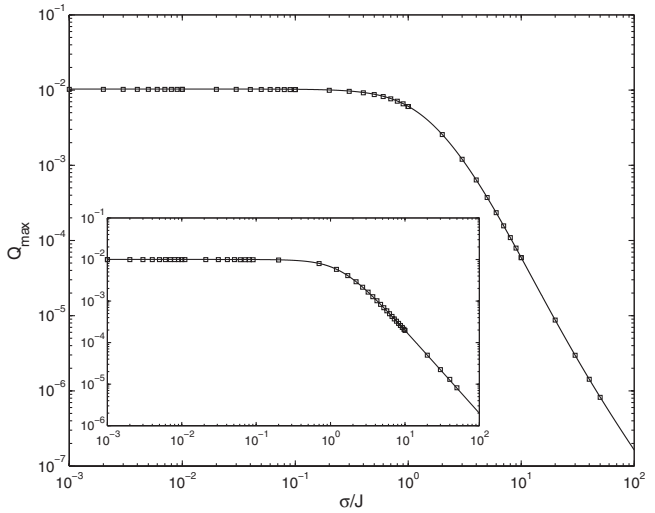

FIG. 5. Maximum value of the observed super-Poissonian peak Q_{max} as a function of the disorder parameter σ. Numerical results (squares) are compared with those obtained from Eq. (22) (solid line). Chosen parameters are $\omega_1 = 10J$, $\Gamma_0 = 2 \times 10^{-2}J$, $\Omega_0 = -1 \times 10^{-3}J$. (Inset) Same as the main plot, but now the energy dependence of the spontaneous decay rates Γ_{ij} is neglected.

could be derived from Eq. (22). By fitting our numerical results, however, we found that also in this case Q_{max} for large inhomogeneity decreases with σ according to a power law: $Q_{max} \propto (\sigma/J)^{-2.65}$. Physically, the observed decrease of super-Poissonian statistics with increasing inhomogeneity (in both models for the decay rates) is a direct consequence of the disorder induced localization of the exciton states. This localization implies that the collective optical properties of the dimer, such as the occurrence of super-Poissonian statistics at $\omega_L \approx \omega_0$, vanish.

To end this section we point out that for laser intensities beyond the small Rabi frequency limit, the effects of disorder on the second order statistics associated with the two-exciton states are qualitatively very similar to those described above. More specific, for small disorder values ($\sigma \ll J$) and laser frequencies $\omega_L = \omega_0$ we may still observe, depending on the intensity of the light, both sub- and super-Poissonian statistics (as found in Fig. 3(b)), because the disorder is too small to destroy the collective nature of the exciton states. In the opposite limit, $\sigma \gg J$, the molecules are effectively almost completely decoupled and, as a result, transitions between super- and sub-Poissonian statistics (at $\omega_L = \omega_0$) will disappear. The statistics in this limit is super-Poissonian, whose magnitude diminishes (grows) with increasing (decreasing) value of the ratio of disorder strength and laser intensity, i.e., σ^2/Ω_0^2.

C. Linear homogeneous trimer

We consider a one dimensional chain consisting of three two-level monomers with equal transition frequencies $\omega_n = \omega_0$ ($n = 1, 2, 3$) and equal transition dipoles ($\boldsymbol{\mu}_1 = \boldsymbol{\mu}_2 = \boldsymbol{\mu}_3$), separated by equal distances. Restricting ourselves to nearest-neighbor interactions J (>0) only and open boundary conditions, diagonalising the 3×3 Hamiltonian matrix (Eq. (1)) yields the one-exciton states, denoted $|1; \rho\rangle$ ($\rho = 1, 2, 3$), and energies $E_{1;\rho}$

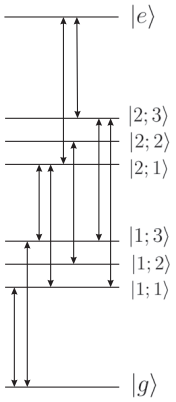

FIG. 6. Level diagram of the linear homogeneous trimer with all molecules having equal transition dipole vectors. The arrows correspond to the optically allowed transitions.

$$
\begin{aligned}
|1;1\rangle &= \frac{1}{2}|1\rangle - \frac{1}{\sqrt{2}}|2\rangle + \frac{1}{2}|3\rangle, \quad & E_{1;1} &= \omega_0 - \sqrt{2}J,\\
|1;2\rangle &= \frac{1}{\sqrt{2}}|1\rangle - \frac{1}{\sqrt{2}}|3\rangle, & E_{1;2} &= \omega_0,\\
|1;3\rangle &= \frac{1}{2}|1\rangle + \frac{1}{\sqrt{2}}|2\rangle + \frac{1}{2}|3\rangle, & E_{1;3} &= \omega_0 + \sqrt{2}J.
\end{aligned}
\tag{23}
$$

Here, $|i\rangle = b_i^\dagger |g\rangle$. The two-exciton states $|2; \sigma\rangle$ ($\sigma = 1, 2, 3$) are found as the Slater determinants of two different one-exciton states $|1; \rho\rangle$ and $|1; \rho'\rangle$ with eigenenergies $E_{2;\sigma} = E_{1;\rho} + E_{1;\rho'}$. Furthermore, the three-exciton state $|e\rangle$ is the state where all three monomers are excited ($E_e = 3\omega_0$). Using Eq. (23), it is a straightforward exercise to determine all Rabi frequencies and spontaneous decay rates of allowed transitions in the trimer, depicted schematically in Fig. 6.

Figure 7 shows the numerical results for $I(\omega_L)$ and $Q(\omega_L)$ in the limit of small Rabi frequency. As is observed, $I(\omega_L)$ consists of two peaks centered around the one-exciton transition frequencies $E_{1;1}$ and $E_{1;3}$. $Q(\omega_L)$, correspondingly, shows the second-derivativelike structure characteristic for two-level monomers, where statistics is sub-Poissonian for resonant laser frequencies. Using the parameters corresponding to the $|g\rangle \rightarrow |1; 1\rangle, |1; 3\rangle$ transitions, we confirmed that indeed the trimer behaves as an effective two-level monomer in these frequency regions. Note that the $|g\rangle \rightarrow |1; 2\rangle$ transition is dipole forbidden, which explains the absence of sub-Poissonian statistics for $\omega_L \approx \omega_0$.

Furthermore, in Fig. 7(b) two super-Poissonian peaks are found at laser frequencies $\omega_L \approx \omega_0 \pm J/\sqrt{2}$, i.e., halfway the transition frequencies of the two-exciton states $|2; 1\rangle$ and $|2; 3\rangle$. As in the case of the dimer, we expect these peaks to result from the direct excitation of the two-exciton states from the ground state by means of a two-photon absorption process followed by the de-excitation to the ground state through the emission of two photons. Thus, with appropriate replacements the peaks should be in perfect agreement with Eq. (22), which was indeed numerically confirmed. We note that similar behavior is not observed for laser frequencies $\omega_L \approx \omega_0$ halfway the transition frequency of the $|2; 2\rangle$ state, because

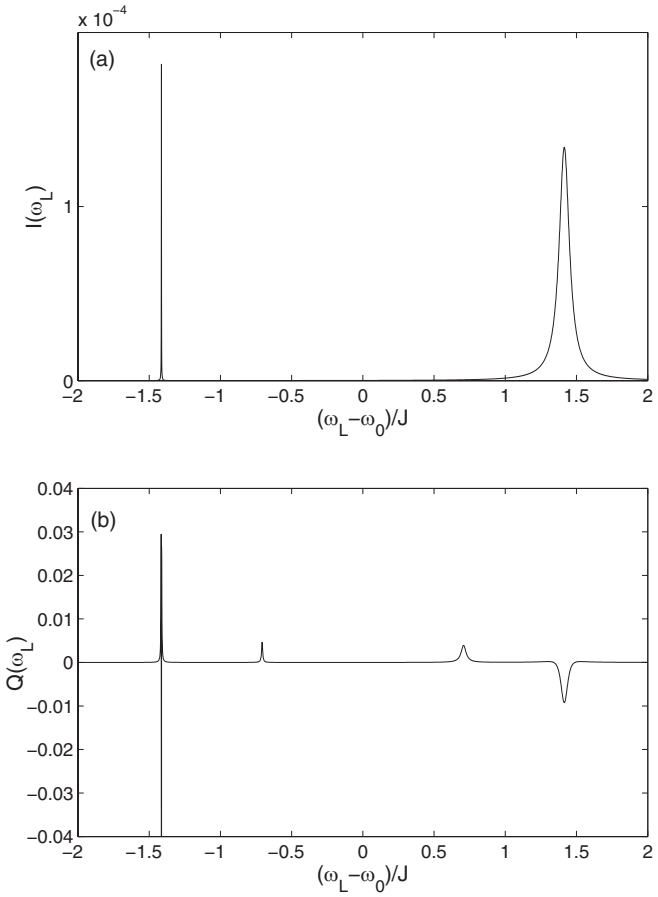

FIG. 7. (a) $I(\omega_L)$ and (b) $Q(\omega_L)$ versus $(\omega_L - \omega_0)/J$ for the homogeneous trimer in the limit of small Rabi frequency. Chosen parameters are $\omega_0 = 10J$, $\Gamma_0 = 2 \times 10^{-2}J$, and $\Omega_0 = -1 \times 10^{-3}J$.

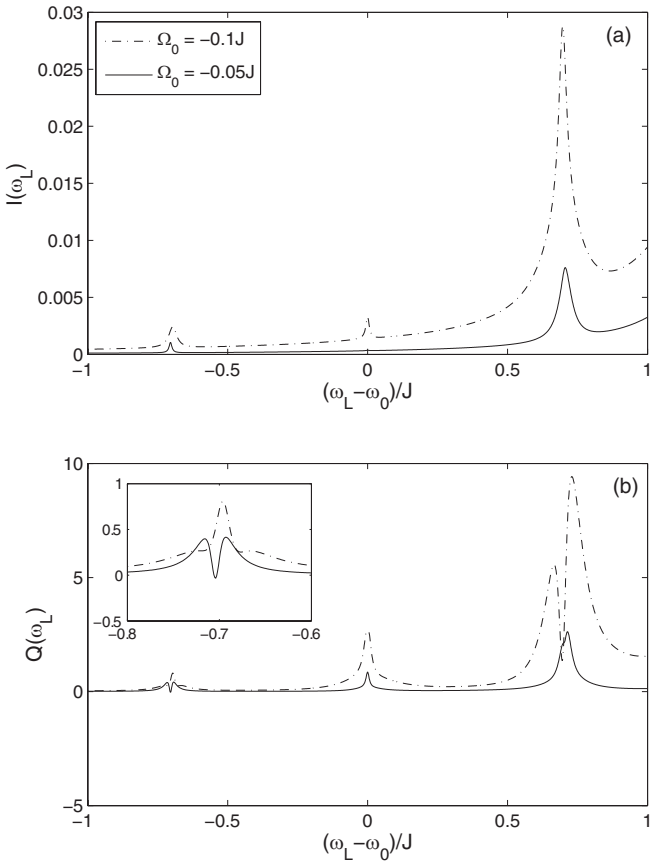

FIG. 8. (a) $I(\omega_L)$ and (b) $Q(\omega_L)$ for the trimer plotted against $(\omega_L - \omega_0)/J$ for $\Omega_0 = -0.05J$ and $-0.1J$. Chosen parameters are the same as those of Fig. 7. The range for ω_L is chosen to reflect the characteristics of multi-exciton influences in more detail. (Inset) Detailed behavior of the frequency regime near $\omega_L = \omega_0 - J/\sqrt{2}$, which is the transition frequency between the ground state and the $|1; 1\rangle$ one-exciton state.

this state cannot be created by any (multi-)photon excitation or emission process.

Figure 8 displays the numerical results for $I(\omega_L)$ and $Q(\omega_L)$ for increasingly fast Rabi oscillations, revealing several characteristics of the influence of multi-exciton states on the photon statistics. For $\omega_L \approx \omega_0 \pm J/\sqrt{2}$, $I(\omega_L)$ in Fig. 8(a) shows the appearance of two new peaks compared to the low Rabi frequency limit. Similar to the dimer case, they result from the increasing occurrence (for increasing laser intensities) of two-photon absorption processes that populate the two-exciton states $|2; 1\rangle$ and $|2; 3\rangle$ and the corresponding decay to the $|g\rangle$ state via one of the one-exciton states. For $\omega_L \approx \omega_0$, a third new peak can be observed in the spectrum, which has no analogue in the dimer case. It originates from the resonance nature of three-exciton creation via a three-photon absorption process, which, at larger Rabi frequencies, significantly populates the $|e\rangle$ state.

As seen in Fig. 8(b), for $\omega_L \approx \omega_0 \pm J/\sqrt{2}$, $Q(\omega_L)$ shows a transition from the Lorentzian super-Poissonian peak shape (as observed in the small Rabi frequency limit) to the second-derivativelike structure. This transition was already encountered for the homogeneous dimer upon increasing laser intensities and gave rise to the sub-Poissonian statistics seen there. Here, for laser frequencies halfway the transition frequency of the $|2; 1\rangle$ state, sub-Poissonian statistics is again observed, although the minimum values of $Q(\omega_L)$ lie closer to zero than in the dimer case, indicating that the sub-Poissonian statistics resulting from the excitation of two-exciton states is less pronounced for the trimer. In fact, for laser frequencies halfway the transition frequency of the $|2; 3\rangle$ state, we do observe the transition to the second-derivativelike structure, but statistics remains super-Poissonian for all laser intensities.

These findings illustrate that for larger aggregates signs of multi-exciton states may still be observed in $Q(\omega_L)$, although interesting characteristics connected with these states, for example the super- to sub-Poissonian transition for resonant laser frequencies, tend to disappear. This results from the rapidly increasing number of (resonant) excitation and decay pathways for larger aggregates, which, in the end, destroys the (anti-)correlations in the photon emission process arising from the multi-exciton states.

For laser frequencies resonant with the three-photon excitation process, i.e., $\omega_L \approx \omega_0$, we observe in Fig. 8(b) a super-Poissonian single peak structure, which can be understood as follows. Once the $|e\rangle$ state is populated, the system rather will decay via the emission of two consecutive photons to one of the one-exciton states than recreate the $|e\rangle$ state through one-photon excitation from the two-exciton state, as the latter process is not resonant with the laser frequency. In the one-exciton state, both the re-excitation (one-photon absorption)

to the two-exciton state (resonant process) and the decay towards the ground state occur; whether one of these pathways dominates the other depends sensitively on the values for the emission constants and Rabi frequencies involved. In the end, however, in both cases the decay from the $|e\rangle$ state gives rise to photon bunching (either from two or from three photons) leading to the observed super-Poissonian statistics.

To corroborate on this further, we expect that this super-Poissonian peak is related to the three-photon absorption line shape, similar to the way in which the two-photon absorption line shape was connected to super-Poissonian behavior of the two-exciton state in the dimer (i.e., see Eqs. (20) and (21)). As a result, the maximum value Q_{max} (at $\omega_L = \omega_0$) of the super-Poissonian peak should scale with increasing laser intensity Ω_0 according to a power law with cubic exponent. Numerical calculation of Q_{max} for different values of the laser intensity (between $\Omega_0 = -5 \times 10^{-3} J$ and $\Omega_0 = -5 \times 10^{-2} J$) revealed that indeed the dependence of Q_{max} on laser intensity obeys a power law. The corresponding exponent was found to be 3.25, which is in good agreement with the expected value of three.

It is interesting to notice that for the Rabi frequencies considered in Fig. 8(b), no transition towards the second-derivativelike structure is (yet) observed in the frequency region $\omega_L \approx \omega_0$, as opposed to the statistics resulting from the two-exciton states. This derives from the fact that higher laser intensities are required to excite the three-exciton state than two-exciton states. This is already apparent from Fig. 7(b), where at low laser intensities no signal was found in $Q(\omega_L)$ at frequencies resonant with the three-photon absorption process, in contrast to the statistics connected with the two-exciton states, which clearly show up at the intensities used there. If the Rabi frequencies are increased even further, we find that also the statistics connected with three-exciton creation undergoes the transition towards a second-derivativelike structure, although possible sub-Poissonian behavior at $\omega_L = \omega_0$ was not observed.

IV. CONCLUSIONS

Using the generating function formalism, we have studied broadband photon emission statistics for small molecular aggregates (Frenkel exciton systems) driven by a monochromatic laser field. This method allows one to extract statistical moments from the set of GBE. Numerically, we found it convenient to invoke the rotating wave approximation as the resulting linear differential equations only have time-independent coefficients. To analyze and explain the results of broadband photon statistics more carefully, we introduced a photon tracking method. This method, based on extending the generating function, allows us to distinguish between photons that originate from different transitions.

The statistical moments of the photon emission process in the limit of long measurement times were obtained numerically in terms of the fluorescence excitation line shape and Mandel's Q parameter for the dimer and the linear homogeneous trimer. Especially, the Q parameter provided interesting information on the role of multi-excitonic states in these systems, even in the limit of low laser intensity. For laser frequencies close to resonance with the transition frequency of a one-exciton state, we found that photon statistics can to a good approximation be reduced to the two-level monomer statistics, although slight deviations occurred for increasing laser intensities. Furthermore, for laser frequencies halfway the transition frequency of a two-exciton state and using low laser intensity, a Lorentzian super-Poissonian peak was observed in the Q parameter. This phenomenon is related to populating the two-exciton state by a resonant two-photon absorption process and the corresponding decay back to the ground state by the rapid emission of two photons (bunching). Interestingly, this peak was found to be in excellent agreement with the ratio between the two-photon absorption line shape and the two-level monomer line shapes. Therefore, information on the two-exciton states in the system can be determined from Q. For increasing laser intensities, a transition from the Lorentzian super-Poissonian peak to a second-derivativelike structure was observed for these laser frequencies. In several cases, this second-derivative structure showed a valley of sub-Poissonian statistics in between two super-Poissonian peaks, a characteristic usually only observed for monomers. We point out that Ω_0/J is used as a measure for the excitation intensity throughout this paper. To connect to experiment, we may express this measure of excitation intensity in absolute units, such as a power per unit area, using the Poynting vector S. Assuming a typical value for the dipole moment of $\mu = 10$ D and a typical interaction strength of $J = 600\ \mathrm{cm}^{-1}$, we found the following relation between the power flux and Ω_0/J: $S \approx 6.8 \times 10^2 \left(\Omega_0^2/J^2\right)\ \mathrm{W}\ \mu\mathrm{m}^{-2}$. Thus, the region of low laser intensities, defined in this paper as $\Omega_0 \leq 10^{-3} J$, translates into $S \lessapprox 0.7\ \mathrm{mW}\ \mu\mathrm{m}^{-2}$ for the power per unit area. High laser intensities of $\Omega_0 = 0.1J$ correspond to $S \approx 7\ \mathrm{W}\ \mu\mathrm{m}^{-2}$.

By studying both the dimer and trimer system, we found that photon statistics of the trimer, although more complex than the dimer, shows the same essential features. In particular, for intermediate laser intensities and exciting with a frequency halfway that of the two-exciton states, we observed the second-derivative structure already encountered in the dimer case, although the valley of sub-Poissonian statistics was less pronounced for the trimer. This finding illustrates that for larger aggregates, detailed characteristics of the emission process associated with multi-exciton states are expected to disappear in the Q parameter. This is a consequence of the increasing number of excitation and decay pathways for larger aggregates, which reduces (anti-)correlations in the photon arrival times. In addition, exploring the role of higher multi-exciton states in large aggregates acquires strong(er) laser illumination. On the other hand, higher order correlations, i.e., higher order moments of $P_n(\omega_L, T)$, may give strong signals even for larger aggregates. This poses an interesting challenge for future research, as such correlations are in general hard to calculate for large aggregates.

ACKNOWLEDGMENTS

We are grateful to Professor R. J. Silbey and Dr. V. A. Malyshev for helpful discussions.

APPENDIX: EIGENSTATES AND GENERALIZED BLOCH EQUATIONS FOR THE DIMER

Consider two two-level monomers with transition frequencies ω_1 and ω_2, respectively, which interact through a resonance dipole-dipole coupling J. For explicitness, we chose J to be positive. Using the Frenkel exciton Hamiltonian of Eq. (5a) we find the one-exciton eigenstates

$$|-\rangle = \frac{1}{\sqrt{1+\eta^2}}[|1\rangle - \eta\,|2\rangle], \qquad |+\rangle = \frac{1}{\sqrt{1+\eta^2}}[\eta\,|1\rangle + |2\rangle]. \tag{A1}$$

Here, $|i\rangle = b_i^\dagger\,|g\rangle$ denotes the state in which only monomer i is excited and $\eta \equiv \frac{E_+ - \omega_2}{J}$, where E_+ is the energy corresponding to the $|+\rangle$ state. The Heitler-London approximation ensures that the dimer ground state $|g\rangle$ is the state where both monomers are in their ground state with energy $E_g = 0$ and that the two-exciton state $|e\rangle$ is the state where both monomers are excited with corresponding energy $E_e = \omega_1 + \omega_2$. The energies corresponding to the one-exciton states are given by

$$E_\pm = \frac{1}{2}\left(\omega_1 + \omega_2 \pm \sqrt{(\omega_1 - \omega_2)^2 + 4J^2}\right). \tag{A2}$$

There are two limiting cases for which Eqs. (A1) and (A2) reduce to a simpler form. In the limit of small inhomogeneity, $\sigma \equiv \left|\frac{\omega_1 - \omega_2}{2}\right| \ll J$, the one-exciton states reduce to those of the homogeneous dimer, $|\pm\rangle = \frac{1}{\sqrt{2}}(|1\rangle \pm |2\rangle)$ with corresponding energies $E_\pm = \omega_0 \pm J$. In the opposite limit of large inhomogeneity, $\sigma \gg J$, the one-exciton states reduce to the excited states of the uncoupled molecules $|i\rangle = b_i^\dagger\,|g\rangle$ with energies ω_1 and ω_2.

To calculate the Rabi frequencies corresponding to the possible transitions, it is assumed for simplicity that the transition dipoles of the monomers have equal magnitude and orientation ($\boldsymbol{\mu}_1 = \boldsymbol{\mu}_2 = \boldsymbol{\mu}$). Using Eq. (4), the Rabi frequencies are given by

$$\Omega_{g\pm} = \Omega_{\pm e} = \frac{\Omega_0}{\sqrt{1+\eta^2}}(1 \pm \eta). \tag{A3}$$

Here, $\Omega_0 \equiv -\frac{\boldsymbol{\mu}\cdot\mathbf{E}_0}{2}$ is the Rabi frequency for a single molecule. The spontaneous decay rates for the possible transitions follow directly from Eq. (6) as

$$\Gamma_{\pm g} = \Gamma_0\left(\frac{E_\pm}{\omega_0}\right)^3 \frac{1}{1+\eta^2}(1 \pm \eta)^2, \qquad \Gamma_{e\pm} = \Gamma_0\left(2 - \frac{E_\pm}{\omega_0}\right)^3 \frac{1}{1+\eta^2}(1 \pm \eta)^2. \tag{A4}$$

Here, $\omega_0 \equiv \frac{\omega_1 + \omega_2}{2}$ is the mean of the two monomer transition frequencies and $\Gamma_0 \equiv \frac{\mu^2}{3\pi\epsilon}(\frac{\omega_0}{c})^3$ is spontaneous decay rate for a monomer with this mean frequency. Thus, Γ_0 may be regarded as a typical monomer spontaneous emission rate.

The Hamiltonian $\hat{H}(t) = \hat{H}_{agg} + \hat{H}_{int}(t)$ for the inhomogeneous dimer interacting with a continuous wave laser field in the exciton basis $\{|g\rangle, |\pm\rangle, |e\rangle\}$ now can be expressed as

$$H(t) = \begin{pmatrix} 0 & 0 & 0 & 0 \\ 0 & E_- & 0 & 0 \\ 0 & 0 & E_+ & 0 \\ 0 & 0 & 0 & \omega_1+\omega_2 \end{pmatrix} + \cos\omega_L t \begin{pmatrix} 0 & \Omega_{g-} & \Omega_{g+} & 0 \\ \Omega_{g-} & 0 & 0 & \Omega_{-e} \\ \Omega_{g+} & 0 & 0 & \Omega_{+e} \\ 0 & \Omega_{-e} & \Omega_{+e} & 0 \end{pmatrix}. \tag{A5}$$

Here, the first term represents the free inhomogeneous dimer, whereas the second term represents its interaction with the laser field. Using Eqs. (8) and (9) we obtain, within the rotating wave approximation, the following set of generalized Bloch equations

$$\dot{C}^+_{g-} = -\frac{\Gamma_{-g}}{2}C^+_{g-} + [\omega_L - E_-]C^-_{g-} - \Omega_{-e}C^-_{ge} - \Omega_{g+}C^-_{-+}, \tag{A6a}$$

$$\dot{C}^+_{g+} = -\frac{\Gamma_{+g}}{2}C^+_{g+} + [\omega_L - E_+]C^-_{g+} - \Omega_{+e}C^-_{ge} + \Omega_{g-}C^-_{-+}, \tag{A6b}$$

$$\dot{C}^+_{-e} = -\frac{\Gamma_{-g} + \Gamma_{e-} + \Gamma_{e+}}{2}C^+_{-e} + [\omega_L - (\omega_1 + \omega_2 - E_-)] \times C^-_{-e} + \Omega_{g-}C^-_{ge} - \Omega_{+e}C^-_{-+}, \tag{A6c}$$

$$\dot{C}^+_{+e} = -\frac{\Gamma_{+g} + \Gamma_{e-} + \Gamma_{e+}}{2}C^+_{+e} + [\omega_L - (\omega_1 + \omega_2 - E_+)] \times C^-_{+e} + \Omega_{g+}C^-_{ge} + \Omega_{-e}C^-_{-+}, \tag{A6d}$$

$$\dot{C}^+_{ge} = -\frac{\Gamma_{e-} + \Gamma_{e+}}{2}C^+_{ge} + [2\omega_L - (\omega_1 + \omega_2)] \times C^-_{ge} - \Omega_{-e}C^-_{g-} - \Omega_{+e}C^-_{g+} + \Omega_{g-}C^-_{-e} + \Omega_{g+}C^-_{+e}, \tag{A6e}$$

$$\dot{C}^+_{-+} = -\frac{\Gamma_{+g} + \Gamma_{-g}}{2}C^+_{-+} - [E_+ - E_-]C^-_{-+} + \Omega_{g+}C^-_{g-} + \Omega_{g-}C^-_{g+} - \Omega_{+e}C^-_{-e} - \Omega_{-e}C^-_{+e}, \tag{A6f}$$

$$\dot{C}^-_{g-} = -\frac{\Gamma_{-g}}{2}C^-_{g-} - [\omega_L - E_-]C^-_{g-} + \Omega_{-e}C^+_{ge} - \Omega_{g+}C^+_{-+} - 2\Omega_{g-}P^-_{-g}, \tag{A6g}$$

$$\dot{C}^-_{g+} = -\frac{\Gamma_{+g}}{2}C^-_{g+} - [\omega_L - E_+]C^+_{g+} + \Omega_{+e}C^+_{ge} - \Omega_{g-}C^+_{-+} + \Omega_{g+}P^-_{e+} - \Omega_{g+}P^-_{-g} - \Omega_{g+}P^+_{e+} + \Omega_{g+}P^+_{g-}, \tag{A6h}$$

$$\dot{C}^-_{-e} = -\frac{\Gamma_{-g} + \Gamma_{e-} + \Gamma_{e+}}{2} C^-_{-e} - [\omega_L - (\omega_1 + \omega_2 - E_-)]C^+_{-e} - \Omega_{g-} C^+_{ge} + \Omega_{+e} C^+_{-+} - \Omega_{-e} P^-_{e+} + \Omega_{-e} P^-_{-g} - \Omega_{-e} P^+_{e+} + \Omega_{-e} P^+_{g-}, \quad \text{(A6i)}$$

$$\dot{C}^-_{+e} = -\frac{\Gamma_{+g} + \Gamma_{e-} + \Gamma_{e+}}{2} C^-_{+e} - [\omega_L - (\omega_1 + \omega_2 - E_+)]C^+_{+e} - \Omega_{g+} C^+_{ge} + \Omega_{-e} C^+_{-+} - 2\Omega_{+e} P^-_{e+}, \quad \text{(A6j)}$$

$$\dot{C}^-_{ge} = -\frac{\Gamma_{e-} + \Gamma_{e+}}{2} C^-_{ge} - [2\omega_L - (\omega_1 + \omega_2)]C^+_{ge} + \Omega_{-e} C^+_{g-} + \Omega_{+e} C^+_{g+} - \Omega_{g-} C^+_{-e} - \Omega_{g+} C^+_{+e}, \quad \text{(A6k)}$$

$$\dot{C}^-_{-+} = -\frac{\Gamma_{+g} + \Gamma_{-g}}{2} C^-_{-+} + [E_+ - E_-]C^+_{-+} + \Omega_{g+} C^+_{g-} - \Omega_{g-} C^+_{g+} + \Omega_{+e} C^+_{-e} - \Omega_{-e} C^+_{+e}, \quad \text{(A6l)}$$

$$\dot{P}^-_{e+} = -\Omega_{g+} C^-_{g+} + \Omega_{-e} C^-_{-e} + 2\Omega_{+e} C^-_{+e} - \frac{1}{2}\Gamma_{e+}(1+s)(P^+_{e+} + P^-_{e+}) - \frac{1}{2}\Gamma_{e-}(P^+_{e+} + P^-_{e+}) + \frac{1}{2}\Gamma_{+g}(P^+_{e+} - P^-_{e+}), \quad \text{(A6m)}$$

$$\dot{P}^-_{-g} = 2\Omega_{g-} C^-_{g-} + \Omega_{g+} C^-_{g+} - \Omega_{-e} C^-_{-e} + \frac{1}{2} s\Gamma_{e-}(P^+_{e+} + P^-_{e+}) - \frac{1}{2} s\Gamma_{+g}(P^+_{e+} - P^-_{e+}) - \frac{1}{2}\Gamma_{-g}(1+s)(P^-_{-g} + P^+_{g-}), \quad \text{(A6n)}$$

$$\dot{P}^+_{e+} = \Omega_{g+} C^-_{g+} + \Omega_{-e} C^-_{-e} - \frac{1}{2}\Gamma_{e+}(1-s)(P^+_{e+} + P^-_{e+}) - \frac{1}{2}\Gamma_{e-}(P^+_{e+} + P^-_{e+}) - \frac{1}{2}\Gamma_{+g}(P^+_{e+} - P^-_{e+}), \quad \text{(A6o)}$$

$$\dot{P}^+_{g-} = -\Omega_{g+} C^-_{g+} - \Omega_{-e} C^-_{-e} + \frac{1}{2} s\Gamma_{e-}(P^+_{e+} + P^-_{e+}) + \frac{1}{2} s\Gamma_{+g}(P^+_{e+} - P^-_{e+}) - \frac{1}{2}\Gamma_{-g}(1-s)(P^-_{-g} + P^+_{g-}). \quad \text{(A6p)}$$

[1] G. D. Scholes and G. Rumbles, Nature Mater. **5**, 683 (2006).
[2] E. E. Jelley, Nature (London) **138**, 1009 (1936); **139**, 631 (1937).
[3] G. Scheibe, Angew. Chem. **49**, 563 (1936); **50**, 212 (1937).
[4] A. Pawlik, S. Kirstein, U. D. Rossi, and S. Dähne, J. Phys. Chem. B **101**, 5646 (1997).
[5] C. Spitz, J. Knoester, A. Ouart, and S. Daehne, Chem. Phys. **275**, 271 (2002).
[6] F. Würthner, T. E. Kaiser, and C. R. Saha-Möller, Angew. Chem., Int. Ed. **50**, 3376 (2011).
[7] H. van Amerongen, L. Valkunas, and R. van Grondelle, *Photosynthetic Excitons* (World Scientific, Singapore, 2000).
[8] G. D. Scholes, G. R. Fleming, A. Olaya-Castro, and R. van Grondelle, Nat. Chem. **3**, 763 (2011).
[9] G. Hadziioannou and G. G. Malliaras, *Semiconducting Polymers: Chemistry, Physics and Engineering* (Wiley-VCH, Weinheim, 2000).
[10] S. de Boer, K. Vink, and D. A. Wiersma, Chem. Phys. Lett. **137**, 99 (1987).
[11] S. de Boer and D. A. Wiersma, Chem. Phys. Lett. **165**, 45 (1990).
[12] H. Fidder, J. Knoester, and D. A. Wiersma, Chem. Phys. Lett. **171**, 529 (1990).
[13] H. Fidder, J. Terpstra, and D. A. Wiersma, J. Chem. Phys. **94**, 6895 (1991).
[14] H. Fidder, J. Knoester, and D. A. Wiersma, J. Chem. Phys. **98**, 6564 (1993).
[15] A. E. Johnson, S. Kumazaki, and K. Yoshihara, Chem. Phys. Lett. **211**, 511 (1993).
[16] K. Minoshima, M. Taiji, K. Misawa, and T. Kobayashi, Chem. Phys. Lett. **218**, 67 (1994).
[17] S. S. Lampoura, C. Spitz, S. Dähne, J. Knoester, and K. Duppen, J. Phys. Chem. B **106**, 3103 (2002).
[18] T. Brixner, J. Stenger, H. M. Vaswani, M. Cho, R. E. Blankenship, and G. R. Fleming, Nature (London) **434**, 625 (2005).
[19] G. S. Engel, T. R. Calhoun, E. L. Read, T. K. Ahn, T. Mancal, Y.-C. Cheng, R. E. Blankenship, and G. R. Fleming, Nature (London) **446**, 782 (2007).
[20] A. G. Dijkstra, T. la Cour Jansen, and J. Knoester, J. Chem. Phys. **128**, 164511 (2008).
[21] P. Kjellberg, B. Brüggemann, and T. Pullerits, Phys. Rev. B **74**, 024303 (2006).
[22] F. Milota, J. Sperling, A. Nemeth, D. Abramavicius, S. Mukamel, and H. F. Kauffmann, J. Chem. Phys. **131**, 054510 (2009).
[23] W. E. Moerner and L. Kador, Phys. Rev. Lett. **62**, 2535 (1989).
[24] M. Orrit and J. Bernard, Phys. Rev. Lett. **65**, 2716 (1990).
[25] H. Z. Lin, Y. X. Tian, K. Zapadka, K. G. Persson, D. Thomsson, O. Mirzov, P. O. Larsson, J. Widengren, and I. G. Scheblykin, Nano Lett. **9**, 4456 (2009).
[26] H. Z. Lin, R. Camacho, Y. Tian, T. E. Kaiser, F. Würthner, and I. G. Scheblykin, Nano Lett. **10**, 620 (2010).
[27] J. Yu, D. Hu, and P. F. Barbara, Science **289**, 1327 (2000).
[28] J. Vogelsang, T. Adachi, J. Brazard, D. A. Vanden Bout, and P. F. Barbara, Nature Mater. **10**, 942 (2011).
[29] M. B. J. Roeffaers, B. F. Sels, H. Uji-i, F. C. De Schryver, P. A. Jacobs, D. E. De Vos, J. Hofkens, Nature (London) **439**, 572 (2006).
[30] A. M. Oijen, M. Ketelaars, J. Köhler, T. J. Aartsma, and J. Schmidt, Science **285**, 400 (1999).
[31] C. Hettich, C. Schmitt, J. Zitzmann, S. Kuhn, I. Gerhardt, V. Sandoghdar, Science **298**, 385 (2002).
[32] J. Hernando, J. P. Hoogenboom, E. M. H. P. van Dijk, J. J. García-López, M. Crego-Calama, D. N. Reinhoudt, N. F. van Hulst, and M. F. García-Parajó, Phys Rev. Lett. **93**, 236404 (2004).
[33] E. Lang, A. Sorokin, M. Drechsler, Y. V. Malyukin, and J. Köhler, Nano Lett. **2635**, 2635 (2005).
[34] E. Barkai, Y. Jung, and R. Silbey, Annu. Rev. Phys. Chem. **55**, 457 (2004).
[35] Y. Jung, E. Barkai, and R. Silbey, J. Chem. Phys. **117**, 10980 (2002).
[36] M. B. Plenio and P. L. Knight, Rev. Mod. Phys. **70**, 101 (1998).
[37] L. Mandel, Opt. Lett. **4**, 205 (1979).
[38] E. Barkai, Y. Jung, and R. Silbey, Phys. Rev. Lett. **87**, 2074031 (2001).
[39] Y. Zheng and F. H. L. Brown, J. Chem. Phys. **119**, 11814 (2003).
[40] Y. Zheng and F. H. L. Brown, Phys. Rev. Lett. **90**, 238305 (2003).
[41] A. Molski, J. Hofkens, T. Gensch, N. Boens, and F. De Schryver, Chem. Phys. Lett. **318**, 325 (2000).
[42] G. C. Hegerfeldt and D. Seidel, J. Chem. Phys. **118**, 7741 (2003).
[43] L. Fleury, M. Segura, G. Zumofen, B. Hecht, and U. P. Wild, Phys. Rev. Lett. **84**, 1148 (2000).
[44] R. Short and L. Mandel, Phys. Rev. Lett. **51**, 384 (1983).
[45] L. Mandel and E. Wolf, *Optical Coherence and Quantum Optics* (Cambridge University Press, 1995).
[46] Y. He and E. Barkai, Phys. Rev. Lett. **93**, 068302 (2004).
[47] Y. Zheng and F. H. L. Brown, J. Chem. Phys. **121**, 7914 (2004).
[48] Y. Zheng and F. H. L. Brown, J. Chem. Phys. **121**, 3238 (2004).

[49]Y. He and E. Barkai, J. Chem. Phys. **122**, 184703 (2005).
[50]S. Jang and R. Silbey, J. Chem. Phys. **118**, 9312 (2003).
[51]S. Jang and R. Silbey, J. Chem. Phys. **118**, 9324 (2003).
[52]F. Sanda and S. Mukamel, J. Chem. Phys. **124**, 1241031 (2006).
[53]A. S. Davydov, *Theory of Molecular Excitons* (Plenum, New York, 1971).
[54]V. M. Agranovich and M. D. Galanin, in *Electronic Excitation Energy Transfer in Condensed Matter*, edited by V. M. Agranovich and A. A. Maradudin (North-Holland, Amsterdam, 1982).
[55]R. J. Cook, Phys. Rev. A **23**, 1243 (1981).
[56]F. L. H. Brown, Acc. Chem. Res. **39**, 363 (2006).
[57]A. Budini, J. Chem. Phys. **126**, 054101 (2007).
[58]G. Bel, Y. Zheng, and F. L. H. Brown, J. Phys. Chem. B **110**, 19066 (2006).
[59]S. Mukamel, Phys. Rev. A **68**, 063821 (2003).
[60]I. Gopich and A. Szabo, J. Chem. Phys. **122**, 014707 (2005).
[61]S. Mukamel, *Principles of Nonlinear Optical Spectroscopy* (Oxford University Press, New York, 1995).
[62]The criterion for the validity of the RWA in case of the dimers and homogeneous trimers discussed in Sec. III are $\frac{\omega_1+\omega_2}{2} \gg \sqrt{\left(\frac{\omega_1-\omega_2}{2}\right)^2 + J^2}$ and $\omega_0 \gg 2\sqrt{2}J$, respectively.
[63]R. W. Boyd, *Nonlinear Optics* (Academic, 2003).